

# Simultaneous microscopic investigation of nozzle internal flow and primary breakup using a transparent high-pressure nozzle

Valeri Kirsch\*, Leif Schumacher, Malte Bieber, Reinhold Kneer, Manuel A. Reddemann  
Institute of Heat and Mass Transfer, RWTH Aachen University, Augustinerbach 6, 52056  
Aachen, Germany

\*Corresponding author: [kirsch@wsa.rwth-aachen.de](mailto:kirsch@wsa.rwth-aachen.de)

## Abstract

A novel transparent direct injection nozzle concept is used to simultaneously visualize nozzle-internal flows and external primary breakup with transmitted light microscopy. Fused silica enables manufacturing of precise 3D internal nozzle geometries with a few micrometer accuracy based on the selective laser etching. To avoid interaction of the metal injector needle with brittle fused silica, a functional separation between nozzle body and nozzle tip is realized. That way, original nozzle body withstands occurring forces (injection pressure, needle forces) while the transparent nozzle tip provides optical access. Simultaneous visualization of nozzle-internal flows and external breakup is obtained by combining an optimized outer nozzle geometry with a compensating glass that equalizes the optical path length between image plane of the microscope and the object plane (inside and outside the nozzle). Recorded images show different internal nozzle phenomena, as for example: i) local liquid-gas interfaces (cavitation structures and entrained air bubbles) indicated by low intensity regions, ii) microscopic flow phenomena (local temperature fluctuations) indicated by schlieren structures, iii) the temporal variation of fuel temperature (presumably by cavitation at needle seat), indicated by the relative refractive index variation between fuel and fused silica. In addition, the relevance of those nozzle internal phenomena for subsequent jet breakup is discussed. For instance jet surface waves that are visible during injection start are connected to boundary-layer instabilities, which are subsequently disturbed by vortex shedding inside the nozzle hole.

## Keywords

automotive spray, primary breakup, microscopy, boundary layer instability, glass nozzle, nozzle flow

## Introduction

Spray development of high-pressure atomizers is strongly influenced by the flow at nozzle outlet. A targeted improvement of mixture formation and subsequent combustion can be achieved by adapting this outlet condition. This goal can only be achieved by a fundamental understanding of nozzle internal flow mechanisms and their influence on breakup phenomena further downstream.

In literature different complementary methods are used to investigate such nozzle internal phenomena and two-phase structures: Large Eddy Simulation and Direct Numerical Simulation [1, 2, 3], high-speed X-ray measurements [4, 5] or optical visualization techniques based on transparent nozzles [6, 7] are the main methods. Analysis of nozzle internal air bubbles [8, 9] or the initial reverse flow during injection start [10] was for instance enabled by such complementary methods. Also the development of cavitation [11, 12, 13, 14], cavitation vortex shedding [15, 16, 17, 18] and ambient gas entrainment into the nozzle at needle closure phase [19, 20] could be observed. However, the impact of nozzle internal conditions on nozzle external phenomena such as mushroom-shaped spray tip formation [21, 22] and transversal waves on jet surfaces [23, 24, 25] have not been fully explored. Also the influence of nozzle internal temperature modulations [26], which should cause change in physical fluid properties and thus influence initial flow structures, is still not fully analyzed.

Using large scaled generic nozzles, the impact of nozzle geometry and even needle movement on spray development can be simultaneously visualized [28, 29, 30]. However, it should be noted that the influence of needle movement and transient flow in real automotive nozzles and injectors can only be approximated with such generic nozzles. Investigations on breakup mechanisms at unscaled and unmodified nozzles can only be applied with the X-ray method that enables simultaneous internal and external nozzle flow visualization. However, significant effort is required for the visualization of small differences in refraction indices inside the liquid or for complex geometries with many overlaid surfaces using x-ray method [27, 28]. For this reasons, conventional microscopy is applied to original sized transparent nozzles. Such transparent nozzles have to fulfill optical accessibility to internal and external flow, while ensuring original nozzle geometry and unmodified injector functionality. In literature it has been established to replace a part of the original nozzle by a transparent part (fused silica, sapphire or acrylic glass). Miranda et al. [29] replaced for instance only a nozzle hole. Alternatively, the entire nozzle tip can be replaced [30, 31, 32, 33]. Either way, the original flow characteristics within the nozzle are not necessarily maintained (difference in edge rounding, k-factor etc.) by replacing the nozzle tip. Even if identical manufacturing processes are used, an exact copy cannot be guaranteed due to production inaccuracies. Therefore in an earlier work, a new manufacturing method based on the selective laser etching technique [34] was established. With this method optical accessibility as well as accuracy of approx. 2  $\mu\text{m}$  is achieved [26]. However, simultaneous observation of internal and external nozzle flow of a single injection was not possible until now due to the difference in the optical path length of approx. 3.2 mm between environment and transparent nozzle. As shown in figure 1, different path lengths result in different focal planes and

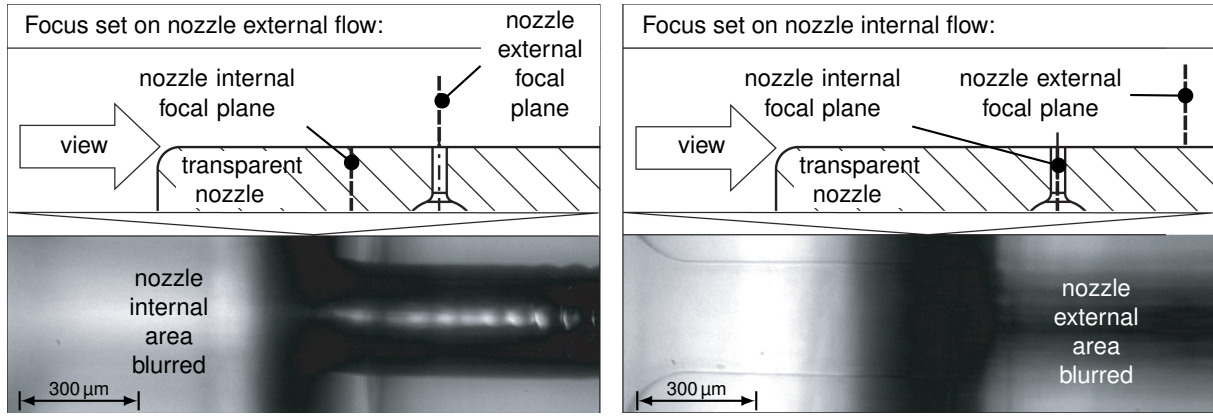


**Figure 1.** Two focus settings without optical path equalization glass and resulting focal planes and single frames of two different high-speed videos showing the same nozzle area. Left: focus is set on the nozzle external flow. Right: focus is set on the nozzle external flow.

therefore in blurring. This circumstances made it impossible to obtain conclusions regarding the effect of individual phenomena on the spray formation.

In this work, an optical path equalization glass, as e.g. used by Busch [35], is established to realize simultaneous visualizations of the internal and external fluid mechanical phenomena. High speed transmitted light microscopy (HS-TLM) is used for imaging at different ambient pressures [36, 26]. Recorded videos deliver highly resolved information of nozzle internal and external breakup mechanisms. Essential understanding of the relationship between nozzle internal and external phenomena can now be gained by these recordings.

### Material and methods

The same setup as used at the work of Kirsch et al. [26] is used to record internal and external nozzle flow. Fig. 2 shows the schematic setup. An equalization glass is added to the nozzle in order to enable simultaneous visualizations of the internal and external nozzle flow. The injector is oriented in such a way that the spray penetrates in direction of gravity into the constant-pressure flow microscopy (CPF-M) vessel [37]. High-speed image series are gained with the high-speed camera “Photron FASTCAM SA-X” with a frame rate of 36 000 fps. The image scale is 620 px/mm, which corresponds to a magnification of 12.4. Illumination is enabled by the laser Cavitar Cavilux Smart. This light source delivers almost monochromatic laser pulses with a pulse duration of  $t_{\text{pulse}} = 10 \text{ ns}$  at a center wavelength of  $\lambda = 640 \text{ nm}$ . Therefore, motion blur and chromatic aberrations are minimized. In addition, speckle patterns can be avoided due to the light source’s short coherence length. Visualization is focused on the transition zone between nozzle interior and the external near nozzle region. Unfortunately, laser polishing produced a rounding with a radius of approx.  $500 \mu\text{m}$  at the edge of the polished surfaces in direction of the nozzle tip, see Kirsch et al. [26] for details. Therefore, a visualization directly at the nozzle hole outlet is not possible due to resulting total reflection. The size of the selected visualized area represent a trade-off between resolution and maximal frame rate. Injection pressure is limited, to  $p_{\text{inj}} = 25 \text{ MPa}$  to avoid nozzle failure. Diesel EN590 is used as fuel and injected with a common automotive pump system (Bosch CP3). Fuel properties and presented dimensionless numbers are shown in table 1. The energizing duration is set to  $t_{\text{en}} = 3 \text{ ms}$ , the ambient pressure to  $p_{\text{amb}} = 0.2 \text{ MPa}$ ,  $p_{\text{amb}} = 0.4 \text{ MPa}$  and  $p_{\text{amb}} = 0.8 \text{ MPa}$  and the ambient temperature to  $T_{\text{amb}} = 293 \text{ K}$ . For each ambient pressure three high-speed videos were taken with a total number of 240 frames.

**Table 1.** Measured diesel (EN590) properties at 293 K and corresponding dimensionless numbers at the investigated ambient pressures.  $p_{\text{amb}}$ .

$\rho$ kg/m <sup>3</sup>	$\eta$ mPa·s	$\sigma$ mN/m	$n$ -	$P_v$ kPa	$p_{\text{amb}}$ MPa	$\rho^*$ -	Re -	Oh -
822	3.71	27.2	1.4574	<1	0.2	2.9e-3	≈16200	≈0.045
					0.4	5.8e-3		
					0.8	11.6e-3		

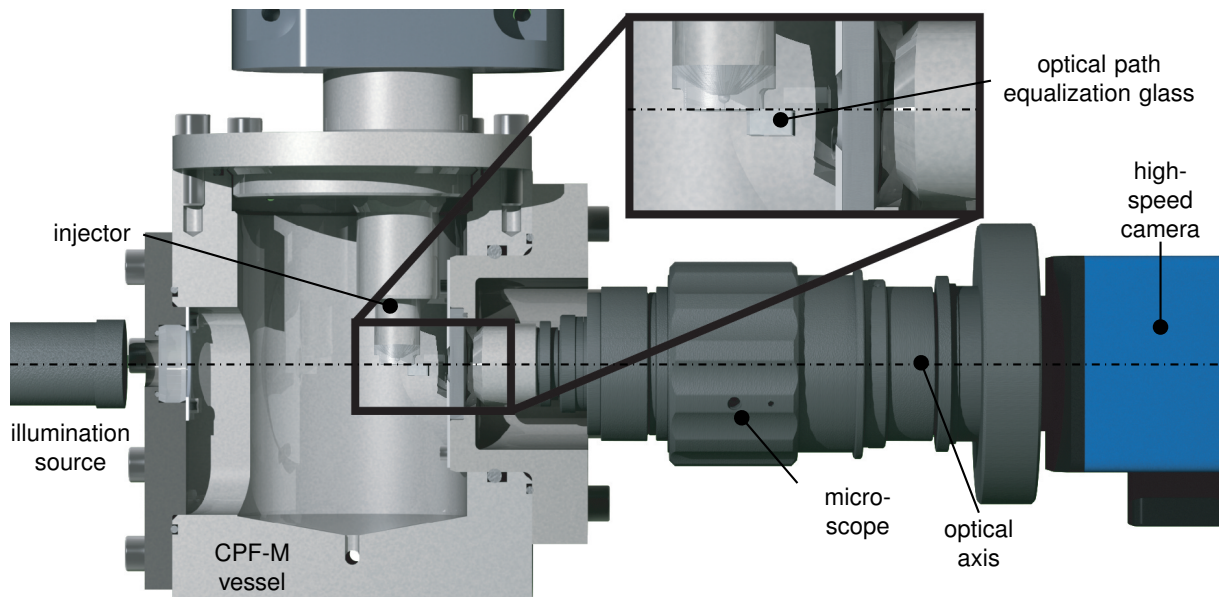


**Figure 2.** Combined setup of the High-Speed Transmitted Light Microscope (HS-TLM) and the Constant-Pressure Flow Microscopy (CPF-M) vessel.

## Results and discussion

Three high-speed videos are shown in figure 3, showing a simultaneous visualization of the nozzle internal and external flow. Each of these videos represents an injection at a specific ambient pressure (top: 0.2 MPa, middle: 0.4 MPa, bottom: 0.8 MPa). First 700  $\mu\text{m}$  of the inner nozzle flow (left) and simultaneously 700  $\mu\text{m}$  of the nozzle external jet (right) are visualized. Even regions close to the liquid-glass interface can be visualized, since injected diesel fuel and surrounding quartz glass have almost identical refractive indices (diesel:  $n = 1.4574$ ; fused silica  $n = 1.4570$ ). First frames (1 to 5) of the videos were not exposed due to a slight time drift between light source and camera.

In the following, various phenomena, structures and observations during injection are described and analyzed. Development of phenomena, such as e.g. air bubbles and their relevance for the injection process, are summarized in paragraphs, therefore chronological order of the injection process is not always given. For a better illustration of single events and observations, hyperlinks to individual frames or frame ranges in Figure 3 are included in the text (framed and marked blue)<sup>1</sup>.

**Air bubble structures and the significance for nozzle-internal and external flow development:** The jet formation during injection start is strongly influenced by occurrence and motion of gas bubbles inside the nozzle. These gas bubbles are trapped in the nozzle hole at the needle closing phase of the previous injection. During injection start, e.g. frame [1](#), such bubbles can be observed as large black structures with a central white area at ambient pressures of 0.4 MPa and 0.8 MPa. For the given nozzle configuration such bubbles are present in approximately 40% of all injections [26] during injection start.

**Bubble formation during injector closing (ambient gas ingestion):** The mechanism of ambient gas ingestion can be described as follows: as soon as the injector needle closes, remaining flow momentum propels fuel out of the nozzle hole. As a consequence, the leaving fuel volume must be replaced by air bubbles that move upstream. Subsequently, the major part of the air is enclosed in the nozzle until the subsequent injection [24], see e.g. frame [2](#) at  $p_{\text{amb}} = 0.2$  MPa, frame [3](#) at  $p_{\text{amb}} = 0.4$  MPa and frame [4](#) at  $p_{\text{amb}} = 0.8$  MPa. However, a part of the entrained air leaves the nozzle already during needle closing. This phenomenon can be observed in the frame range from [6](#) to [10](#) for the ambient pressure of  $p_{\text{amb}} = 0.8$  MPa. As it can be observed, some air bubbles flow in the direction of the nozzle outlet and at the same time, a large ligament is formed directly at nozzle orifice. In this ligament small air bubbles (small round black structures) are trapped.

**Bubbles surface displacement:** The movement of gas bubbles inside the nozzle are indicating the flow field during injection start. As shown in frames [11](#) to [15](#), the air bubbles move first in sac-hole direction, which can be explained by a local low pressure due to needle lifting [26]. Subsequently, during the acceleration phase, the bubbles convex meniscus faced to the sac-hole is deformed to a mostly flat shape. This can be explained by the flow development within the hole in ambient direction. At this early injection time the flow velocities are still low ( $v \approx 10$  m/s). Consequently, the flow is laminar ( $Re = 665$ ) and has a parabolic velocity profile [38]. The parabolic velocity is faced against the convex meniscus and thus the convex shape is reducing with time (frame [16](#) at ambient pressure of 0.4 and 0.8 MPa in figure 3). Furthermore, at an ambient pressure of 8 MPa strong deformation of the bubble even causes a bubble decomposition close to the boundary-layer of the nozzle hole (frame [17](#), close

<sup>1</sup>Hyperlinks and videos are only working with Adobe Reader version 9 or higher, but not greater than 9.4.1 on Linux and Foxit Reader (Flash, video, audio). Furthermore, javascripts need to be enabled. May 29, 2019

Ambient pressure:  $p_{\text{amb}} = 0.2 \text{ MPa}$

Ambient pressure:  $p_{\text{amb}} = 0.4 \text{ MPa}$

Ambient pressure:  $p_{\text{amb}} = 0.8 \text{ MPa}$

**Figure 3.** Three high-speed videos of three different injections using the new optical length correction glass. Injection pressure is 25 MPa, ambient pressure 0.2 MPa (top), 0.4 MPa (middle) and 0.8 MPa (bottom). An energizing time of 3 ms was used.

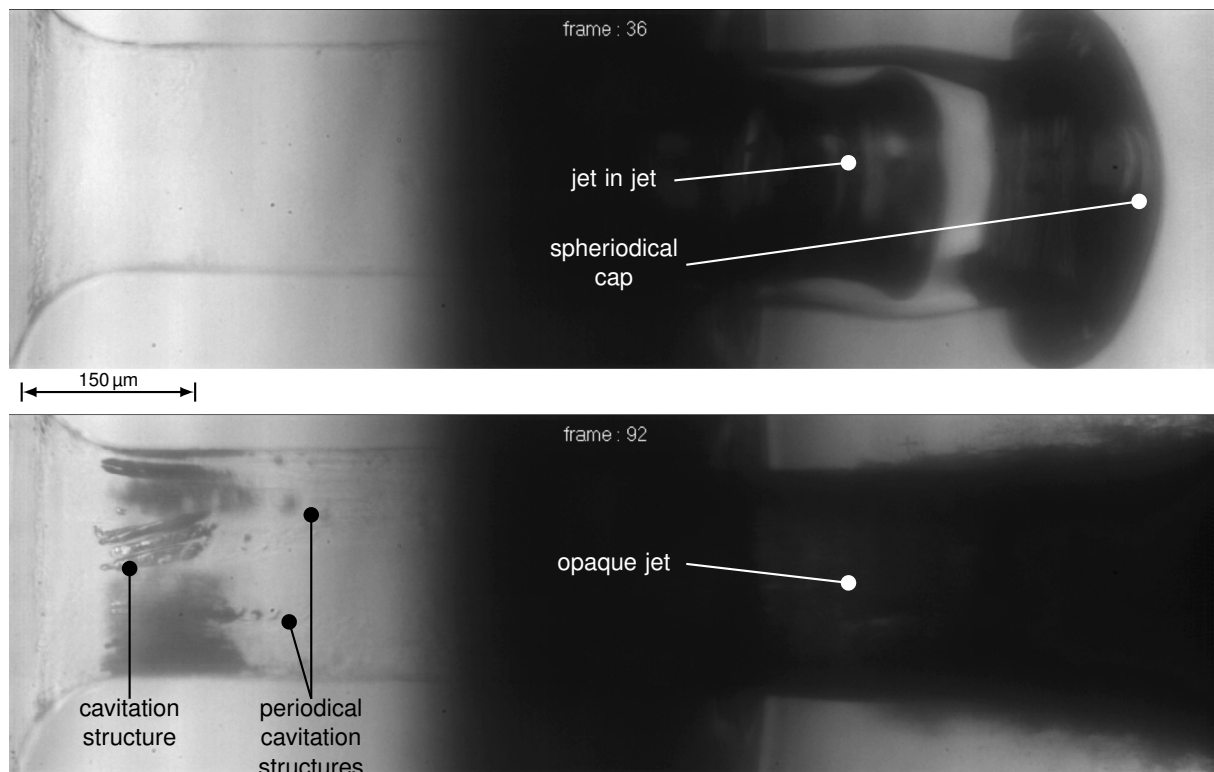


**Figure 4.** Two single frames of the video showing an injection at an ambient pressure of 0.8 MPa. In the frame 36 (top) an “jet in jet” and in frame 92 (bottom) typical cavitation structures at the nozzle hole inlet are shown.

to the invisible area between nozzle hole and ambience). Subsequently at the ambience, a secondary jet inside the main jet can develop (“jet in jet”) by such bubble deformation, visible in figure 4, top or in frame at an ambient pressure of 0.8 MPa in figure 3.

**Pre-ligament jet formation:** Normally, spheroidal caps develop due to aerodynamic shear forces at the penetrating jet tip [24, 22, 21, 35, 4, 16, 39]. Nevertheless, in many investigation pre-ligaments or other structures are also observed instead [21, 4, 24, 33]. The previously described jet in jet phenomenon could be the reason for such observed pre-ligaments in front of the main jet. Crua et al. [22] suggests that such a jet in the slipstream of the main jet penetrates through the spherical cap and thus may generate the observed pre-ligaments. Unfortunately, the area in which such phenomena could be observed is located downstream of the visualized region.



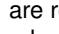
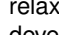
**Fragmentation and entrainment of in the sac-hole accumulated gas:** Besides the large gas bubbles in the nozzle hole, further gas is accumulated in the sac-hole at the needle seat. This gas flows through the visible area after the large gas bubbles in the nozzle hole have left the nozzle, but before reaching the quasi steady injection state. Due to increased flow velocities and resulting shear stresses, these bubbles are entrained and fragmented, see for instance frames . While propagating through the nozzle hole, these bubbles seem to be deformed, by means of expansion or compression, see e.g. frame at  $p_{amb} = 0.2$  MPa, frame at  $p_{amb} = 0.4$  MPa and frame at  $p_{amb} = 0.8$  MPa. Such deformation may be a result of static pressure fluctuations in radial and axial direction. In order to give a profound explanation, records with increased temporal resolution are required.

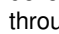
**Fuel cooling by ambient gas:** After injection is completed, moving schlieren structures between nozzle and sac-hole indicate a variation in density, see e.g. in figure 3 frame range from at all ambient pressures. According to Settles [40], a shadow image show intensity modulations related to the second spatial derivation of the refractive index. The here presented schlieren structure, thus indicates a refractive index difference between sac- and nozzle hole. The bright fringes of the observed schlieren structure, appear on the sac-hole side, while the dark fringes appear on the nozzle hole side. Thus, the refractive index increases from sac- to nozzle hole side, which in turn means that the density increases in the same direction [22]. A possible reason for such density increase is a temperature decrease from sac- to nozzle hole side. A temperature variation in between is only possible if fuel and ambient gas variate in temperature. During the end of injection, the gas/liquid ratio inside the nozzle hole is higher. Consequently, the temperature of the ambient gas has to be lower compared the fuel temperature. Over time, the temperatures equalize and the observed schlieren structures vanish.

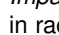
**Fuel cooling by ambient gas:** After injection is completed, moving schlieren structures between nozzle and sac-hole indicate a variation in density, see e.g. in figure 3 frame range from at all ambient pressures. According to Settles [40], a shadow image show intensity modulations related to the second spatial derivation of the refractive index. The here presented schlieren structure, thus indicates a refractive index difference between sac- and nozzle hole. The bright fringes of the observed schlieren structure, appear on the sac-hole side, while the dark fringes appear on the nozzle hole side. Thus, the refractive index increases from sac- to nozzle hole side, which in turn means that the density increases in the same direction [22]. A possible reason for such density increase is a temperature decrease from sac- to nozzle hole side. A temperature variation in between is only possible if fuel and ambient gas variate in temperature. During the end of injection, the gas/liquid ratio inside the nozzle hole is higher. Consequently, the temperature of the ambient gas has to be lower compared the fuel temperature. Over time, the temperatures equalize and the observed schlieren structures vanish.

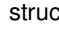
**Cavitation structures and the significance for nozzle-internal and external flow development:** Small black structures, which appear at the transition region between sac-hole and the nozzle hole and expand in downstream direction, are classified as cavitation structures, see for instance figure 3 frame at all ambient pressures or figure 4. Minimum static pressure in the nozzle is achieved at the end of this transition zone. Thus, at this axial position static pressure drops below the vapor pressure and cavitation structures develop [38, 41]. Surface defects

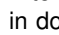

at the circumferential line at the end of the transition zone are most likely acting as cavitation seeds. Therefore, origins of such cavitation structures on the nozzle hole inlet surface in azimuthal direction remain always the same. Due to a short depth of field of the microscope local cavitation structures can be attributed to the azimuthal locations. Thereby, the amount of cavitation on a circumferential line could be qualitatively estimated. However, a quantitative statement as a function of ambient pressure and/or time is hardly possible due to the lack of measurement data.

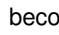
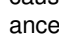
Before cavitation takes place, formation of wave structures on the free jet surface can be observed for instance in frame  at  $p_{amb} = 0.2$  MPa, frame  at  $p_{amb} = 0.4$  MPa and frame  at  $p_{amb} = 0.8$  MPa. Such waves are related to boundary-layer instabilities [24]. Boundary-layer instabilities are developing, due to jet velocity profile relaxation after the jet penetrates into chamber ambients [42, 43]. However, shortly after such boundary-layer waves develop, a significant change of the jet appearance can be observed, see e.g. frame  at all ambient pressures. The jet core no longer appears smooth, structured, with a glare line on the jet axis and surface waves on it, but becomes opaque and a large number of small structures (ligaments and droplets) around it become noticeable. Such an appearance indicates increased turbulence in the boundary-layer of the nozzle internal flow. Cavitation at this time period is still not visible, only above described fragmented air bubbles are present.

*Cavitation vortex shedding:* Therefore, cavitation can not be the reason for occurring turbulences. To find an reasonable explanation for the increased turbulence subsequent cavitation structures are analyzed: A periodical development of cavitation bubbles downstream of the vena contracta can be observed. This periodicity is visible through an equal distance between cavitation structures in flow direction, see e.g. figure 4 or figure 3 frame . These periodical cavitation appearance is called cavitation vortex shedding [15, 16, 17, 18]. Generally, vortex shedding is initialized by the flow around the nozzle hole inlet rounding between sac- and nozzle hole at certain velocities. Vortex shedding, which is present in this work, becomes visible only due to the development of cavitation structures inside the vortexes. Even initial vortex shedding, without the appearance of cavitation structures, initialize turbulence in the nozzle hole and disturbs the boundary-layer. Such invisible vortex shedding can therefore result in the observed opaque jet surface with small ligaments and droplets around the jet. Cavitation during the cavitation vortex shedding appearance only enhances such turbulence.

*Impact of cavitation on nozzle internal vortex:* Due to the expansion of occurring cavitation structures in axial and in radial direction, a tangential velocity share can be assumed in the nozzle hole, see e.g. figure 3 frame  or figure 4, button. Such a tangential velocity share indicates a vortex flow inside the nozzle hole and can be caused by string cavitation inside the sac hole [12, 13] or by an off-centered needle position [44]. In this work no string cavitation is visible therefore an off-centered needle position is most likely the reason for occurring vortexes.

*Cavitation bubbles appearance and expand:* In this work, quasi steady-state phase is defined when cavitation structures no longer disappear until the nozzle closes. At an ambient pressure of 0.2 MPa in the frame range  multiple small cavitation structures with short life span are visible. These cavitation structures are not used for the definition of the quasi steady-state phase. However, the formation of such cavitation will be shortly discussed in the following. Compared to higher ambient pressures, the throttling of the nozzle hole must be increased at lower ambient pressures. Thus the probability of a static pressure drop below the vapour pressure due to vortex shedding at low ambient pressures is also increased. However, this cavitation development does not stabilize until a certain needle lift.

After cavitation development is stabilized, the cavitation gas bubble extent initially increase from nozzle hole inlet in downstream direction, see frame range from  in figure 3. Subsequently, during nozzle closing, the extent decreases in opposite direction. Temporarily, the cavitation extent most likely reaches the nozzle orifice and forms therefore supercavitation. Such supercavitation should influence the global spray appearance significantly [11]. Unfortunately, global spray appearance can not be shown in this work due to the small visualized area, see for instance in figure 3 frame  at all ambient pressures.

*Fuel heating due to cavitation appearance:* With the appearance of cavitation structures, also schlieren structures become visible downstream of the cavitation. In figure 3 frame  at all ambient pressures such schlieren structures can be observed. These schlieren structures presumably arise from local temperature inhomogeneities, caused by cavitation implosion [45, 26]. In addition, during injection a change in sac and nozzle hole edge appearance is noticeable, see frame range  at each video. This effect can be explained again by refractive index change, presumably caused by varying fuel temperature. Since the edges become less visible, the refractive indices between fused silica and diesel equalize. Fuel temperature should therefore increase, which is in agreement with findings regarding paragraph “fuel cooling by ambient air”. Such a global temperature increase is also potentially caused by cavitation formation between needle and needle seat and subsequent imploding cavitation bubbles [35].

**Quantitative temporal injector behavior:** In figure 5 three different characteristic time events are compared as a function of ambient pressure: i) time until fuel leaves the nozzle, ii) time until stabilized cavitation appear and iii) time until ambient air entrainment occurs. This events can be used as indicators for the temporal injector behavior. Visible trends with increasing ambient pressure will be described and analyzed in the following.

*Injector Opening (Indicated by jet penetration start):* The time until fuel leaves the nozzle decreases slightly with increasing ambient pressure. This effect can be explained by additional pressure forces applied on the needle with increased ambient pressures. This additional force acts in opposite direction to nozzle closing forces and therefore reduces the force required to lift the needle and thus the opening time.

*Quasi steady state (Indicated by stabilized cavitation):* Although less potential exists between high-pressure system and environment with increasing ambient pressure, the average time decreases until stabilized above described cavitation structures occur. A possible explanation for such a behavior could be that the needle opening occurs

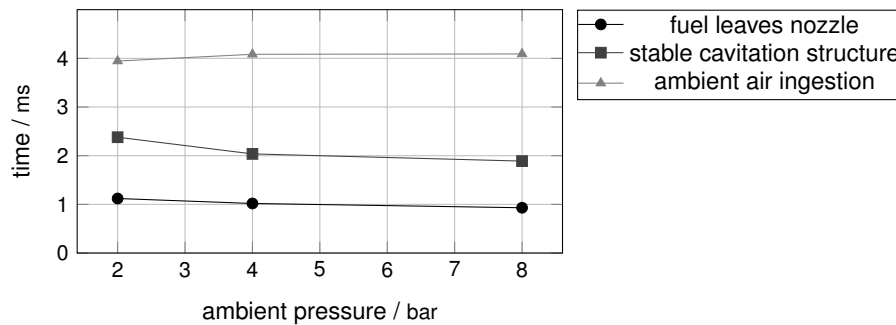


**Figure 5.** Observed characteristic injection time events as function of the ambient pressure: Time until fuel leaves the nozzle orifice, time until a stable cavitation is developed and time until air ingestion. Shown times are averaged times of the three videos.

earlier and thus the time until the stabilized cavitation structures occur decreases in the same order of magnitude. Yet, the mean time between needle opening and the appearance of stable cavitation structures decreases from  $\Delta t = 1.26$  ms at  $p_{\text{amb}} = 0.2$  MPa to  $\Delta t = 1.02$  ms at  $p_{\text{amb}} = 0.4$  MPa to  $\Delta t = 0.96$  ms at  $p_{\text{amb}} = 0.8$  MPa. Therefore, an earlier appearance of stable cavitation cannot be explained by the earlier needle opening alone. An additional reduction in time can only be caused if the needle not only opens earlier but also accelerates faster with increasing ambient pressure. In short, the elevated ambient pressure increase the force on the needle and additionally reduces the pressure difference between fuel supply system and ambience. Following the Newton's second law of motion, the acceleration of an object increases with increasing force acting on it. Therefore, initial higher ambient pressure causes an accelerated needle lifting.

*Injector closure (Indicated by ambient air entrainment):* In this work, needle closure is indicated with ingestion of ambient air. A clear statement regarding the closing behavior of the nozzle as a function of the ambient pressure cannot be made, see figure 5. Either way, the time between end of supercavitation and ingestion of ambient air ( $\Delta t \approx 0.25$  ms) is much shorter than the time between start of jet penetration into ambience and development of the quasi steady-state cavitation structures ( $\Delta t \approx 1.1$  ms). These time differences can be used as a benchmark for needle closing and opening speed. The difference in time between opening and closing results from higher needle closing forces compared to needle opening forces. The built-in spring inside the injector not only keeps the needle closed when not actuated, but acts also against needle opening forces during the injection. Therefore, needle acceleration at the end of injection is due to sum of pressure and spring force much higher and consequently nozzle closing requires less time compared to the nozzle opening.

## Summary

In this work, a first previously manufactured transparent nozzle [26] was used for enhanced analysis of nozzle internal and external phenomena occurring during injection. A simultaneous visualization of the nozzle internal and external phenomena is achieved using an optical path equalization glass. On this basis local and global effects such as ambient gas entrainment and cavitation and the relevance of those for nozzle-internal and external flow development were analyzed in detail. As a result, it was shown that entrained ambient gas in the nozzle has great influence on jet tip development. This entrained air leads for instance to observed phenomena like a "jet in jet" or also in literature observed pre-ligaments. It was also found that cavitation in this work is not the main reason for opaque jet appearances, but boundary-layer turbulences caused by vortex shedding at the nozzle hole inlet. Occurring cavitation structures are only enhancing these disturbances but have a great influence on local and global fuel temperature inside the nozzle.

## Acknowledgement

This work was funded by the Deutsche Forschungsgemeinschaft (DFG, German Research Foundation) under Germany's Excellence Strategy – Cluster of Excellence 236 "Tailor-Made Fuels from Biomass" - ID: 39030946 and Cluster of Excellence 2186 "The Fuel Science Center" - ID: 390919832.

The help of Jonathan Scheu and Florian Werner Müller (student assistants) during nozzle and optical path equalization glass design are gratefully acknowledged by the authors.

## References

- [1] Ferziger, J. H., and Perić, M., eds., 1999. *Computational methods for fluid dynamics*, 2. rev. ed. ed. Springer Verlag, Berlin.
- [2] Baumgarten, C., Shi, Y., Busch, R., and Merker, G. P., 2001. In ILASS - Europe 2001, European Conference on Liquid Atomization and Spray Systems, 2 –6 September 2001, Zürich, Switzerland.
- [3] Bode, M., Deshmukh, A., Kirsch, V., Reddemann, M. A., Kneer, R., and Pitsch, H., 2015. In ICLASS 2015, 13th Triennial International Conference on Liquid Atomization and Spray Systems, Tainan, Taiwan, August 23-27, 2015.
- [4] Liu, Z., Im, K.-S., Wang, Y., Fezzaa, K., Xie, X.-B., Lai, M.-C., and Wang, J., 2010. In SAE 2010 World Congress & Exhibition.

- [5] Moon, S., Gao, Y., Park, S., Wang, J., Kurimoto, N., and Nishijima, Y., 2015. *Fuel*, **150**, pp. 112–122.
- [6] Blessing, M., König, G., Krüger, C., Michels, U., and Schwarz, V., 2003. In SAE 2003 World Congress & Exhibition.
- [7] Watanabe, H., Nishikori, M., Hayashi, T., Suzuki, M., Kakehashi, N., and Ikemoto, M., 2015. *International Journal of Engine Research*, **16**(1), pp. 5–12.
- [8] Blessing, M., 2004. PhD thesis, University of Stuttgart, Stuttgart.
- [9] Ghiji, M., Goldsworthy, L., Brandner, P. A., Garaniya, V., and Hield, P., 2016. In AFMC 2016.
- [10] Badock, C., 1999. PhD thesis, TU Darmstadt, Darmstadt.
- [11] Chaves, H., Knapp, M., Kubitzek, A., Obermeier, F., and Schneider, T., 1995. In International Congress and Exposition.
- [12] Gavaises, M., and Andriotis, A., 2006. In 2006 SAE World Congress.
- [13] Papoulias, D., Giannadakis, E., Mitroglou, N., Gavaises, M., and Theodorakakos, A., 2007. In 2007 World Congress.
- [14] Bornschlegel, S., Conrad, C., Durst, A., Wang, J., and Wensing, M., 2018. *International Journal of Engine Research*, **19**(1), pp. 67–77.
- [15] Sou, A., and Pratama, R. H., 2016. *Atomization and Sprays*, **26**(9), pp. 939–959.
- [16] Hult, J., Simmank, P., Matlok, S., Mayer, S., Falgout, Z., and Linne, M., 2016. *Experiments in Fluids*, **57**(4), p. 49.
- [17] Mitroglou, N., Stamboliyski, V., Karathanassis, I. K., Nikas, K. S., and Gavaises, M., 2017. *Experimental Thermal and Fluid Science*, **84**, pp. 179–189.
- [18] Mashida, M., and Sou, A., 2018. *International Journal of Automotive Engineering*, **9**(1), pp. 9–15.
- [19] Battistoni, M., Poggiani, C., and Som, S., 2016. *SAE International Journal of Engines*, **9**(1).
- [20] Ghiji, M., Goldsworthy, L., Brandner, P., Garaniya, V., Hield, P., and Brandner, P. A., 2018. *Atomization and Sprays*, **28**(1), pp. 23–45.
- [21] Badock, C., Wirth, R., Fath, A., and Leipertz, A., 1999. *International Journal of Heat and Fluid Flow*, **20**(5), pp. 538–544.
- [22] Crua, C., Heikal, M. R., and Gold, M. R., 2015. *Fuel*, **157**, pp. 140–150.
- [23] Kirsch, V., Reddemann, M. A., Palmer, J., and Kneer, R., 2017. *Atomization and Sprays*, **27**(9), pp. 791–805.
- [24] Kirsch, V., Reddemann, M. A., Palmer, J., and Kneer, R., 2017. In ILASS - Europe 2017, 28th Annual Conference on Liquid Atomization and Spray Systems, 6-8 Sep. 2017, Valecia, Spain.
- [25] Shinjo, J., Xia, J., and Umemura, A., 2015. *Proceedings of the Combustion Institute*, **35**(2), pp. 1595–1602.
- [26] Kirsch, V., Hermans, M., Schönberger, J., Ruoff, I., Willmann, M., Reisgen, U., Kneer, R., and Reddemann, M. A., 2019. *Review of Scientific Instruments*, **90**.
- [27] Linne, M., 2012. *Experiments in Fluids*, **52**(5), pp. 1201–1218.
- [28] Linne, M., 2013. *Progress in Energy and Combustion Science*, **39**(5), pp. 403–440.
- [29] Miranda, R., Chaves, H., and Obermeier, F., 2002. In ILASS - Europe 2002, 18th Annual Conference on Liquid Atomization and Spray Systems, 9–11 September 2002, Zaragoza, Spain.
- [30] Miranda, R., Chaves, H., Martin, U., and Obermeier, F., 2003. In ICLASS 2003, 9th Triennial International Conference on Liquid Atomization and Spray Systems, September 13-17, 2003, Sorrento, Italy.
- [31] Hayashi, T., Suzuki, M., and Ikemoto, M., 2013. *International Journal of Engine Research*, **14**(6), pp. 646–654.
- [32] Mamaikin, D., Knorsch, T., Rogler, P., Leick, P., and Wensing, M., 2017. In ILASS - Europe 2017, 28th Annual Conference on Liquid Atomization and Spray Systems, 6-8 Sep. 2017, Valecia, Spain.
- [33] Manin, J., Pickett, L. M., and Yasutomi, K., 2018. In ICLASS 2018, 14th Triennial International Conference on Liquid Atomization and Spray Systems, Chicago, IL, July 22-26, 2018.
- [34] Hermans, M., 2014. *Journal of Laser Micro/Nanoengineering*, **9**(2), pp. 126–131.
- [35] Busch, R., 2001. PhD thesis, Hochschule Hannover, Hannover.
- [36] Kirsch, V., Reddemann, M. A., Thalheim, B., Palmer, J., and Kneer, R., 2016. In 4th TMFB International Conference, Aachen, Germany, 21-23 June 2016.
- [37] Reddemann, M. A., Kirsch, V., and Kneer, R., 2014. In ILASS – Europe 2014, 26th Annual Conference on Liquid Atomization and Spray Systems, 8-10 Sep. 2014, Bremen, Germany.
- [38] Siekmann, H. E., and Thamsen, P. U., eds., 2008. *Strömungslehre: Grundlagen ; mit 3 Tabellen*, 2., aktualisierte Aufl. ed. Springer-Lehrbuch. Springer, Berlin.
- [39] Schugger, C., 2007. PhD thesis, RWTH Aachen University, Aachen.
- [40] Settles, G. S., 2001. *Schlieren and Shadowgraph Techniques*. Springer Berlin Heidelberg, Berlin, Heidelberg.
- [41] Chaves, H., Knapp, M., Kubitzek, A., and Obermeier, F., 1993. In Laser Anemometry: Advances and Applications—Fifth International Conference.
- [42] Brennen, C., 1970. *Journal of Fluid Mechanics*, **44**(01), p. 33.
- [43] Yoon, S. S., and Heister, S. D., 2003. *Atomization and Sprays*, **13**(5-6), pp. 499–516.
- [44] Oda, T., Iwatani, T., Takahashi, N., Sumi, T., and Ohsawa, K., 2014. In ILASS – Europe 2014, 26th Annual Conference on Liquid Atomization and Spray Systems, 8-10 Sep. 2014, Bremen, Germany.
- [45] Merouani, S., Hamdaoui, O., Rezgui, Y., and Guemini, M., 2014. *Ultrasonics sonochemistry*, **21**(1), pp. 53–59.